Research Article | Vol. 26, No. 13 | 25 Jun 2018 | OPTICS EXPRESS 16505
Optics EXPRESS

Design rules for optimizing unipolar coded Brillouin optical time-domain analyzers

ZHISHENG YANG,[1,*] ZONGLEI LI,[1,2] SIMON ZASLAWSKI,[1] LUC THÉVENAZ,[1] AND MARCELO A. SOTO[1,3]

[1]*EPFL Swiss Federal Institute of Technology, Institute of Electrical Engineering, SCI STI LT, Station 11, CH-1015 Lausanne, Switzerland*
[2]*Center for Information Photonics & Communications, School of Information Science & Technology, Southwest Jiaotong University, Chengdu, Sichuan, 610031, China*
[3]*Department of Electronic Engineering, Universidad Técnica Federico Santa María, 2390123 Valparaíso, Chile*
**zhisheng.yang@epfl.ch*

Abstract: The performance of unipolar unicolor coded Brillouin optical time-domain analysis (BOTDA) is evaluated based on both Simplex and Golay codes. Four major detrimental factors that limit the system performance, including decoded-gain trace distortion, coding pulse power non-uniformity, polarization pulling and higher-order non-local effects, are thoroughly investigated. Through theoretical analysis and an experimental validations, solutions and optimal design conditions for unipolar unicolor coded BOTDA are clearly established. First, a logarithmic normalization approach is proposed to resolve the linear accumulated Brillouin amplification without distortion. Then it is found out that Simplex codes are more robust to pulse power non-uniformity compared to Golay codes; whilst the use of a polarization scrambler must be preferred in comparison to a polarization switch to mitigate uncompensated fading induced by polarization pulling in the decoded traces. These optimal conditions enables the sensing performance only limited by higher-order non-local effects. To secure systematic errors below 1.3 MHz on the Brillouin frequency estimation, while simultaneously reaching the maximum signal-to-noise ratio (SNR), a mathematical model is established to trade-off the key parameters in the design, i.e., the single-pulse Brillouin amplification, code length and probe power. It turns out that the optimal SNR performance depends in inverse proportion on the value of maximum single-pulse Brillouin amplification, which is ultimately determined by the spatial resolution. The analysis here presented is expected to serve as a quantitative guideline to design a distortion-free coded BOTDA system operating at maximum SNR.

OCIS codes: (060.2370) Fiber optics sensors; (290.5900) Scattering, stimulated Brillouin; (060.4370) Nonlinear optics, fibers.

References and links

1. T. Horiguchi, K. Shimizu, T. Kurashima, M. Tateda, and Y. Koyamada, "Development of a distributed sensing technique using Brillouin scattering," J. Lightwave Technol. **13**(7), 1296–1302 (1995).
2. M. A. Soto and L. Thévenaz, "Modeling and evaluating the performance of Brillouin distributed optical fiber sensors," Opt. Express **21**(25), 31347–31366 (2013).
3. M. Alem, M. A. Soto, and L. Thévenaz, "Analytical model and experimental verification of the critical power for modulation instability in optical fibers," Opt. Express **23**(23), 29514–29532 (2015).
4. S. M. Foaleng and L. Thévenaz, "Impact of Raman scattering and modulation instability on the performances of Brillouin sensors," Proc. SPIE **7753**, 77539V (2011).
5. A. Domínguez-López, X. Angulo-Vinuesa, A. López-Gil, S. Martín-López, and M. González-Herráez, "Non-local effects in dual-probe-sideband Brillouin optical time domain analysis," Opt. Express **23**(8), 10341–10352 (2015).
6. A. Domínguez-López, Z. Yang, M. A. Soto, X. Angulo-Vinuesa, S. Martín-López, L. Thévenaz, and M. González-Herráez, "Novel scanning method for distortion-free BOTDA measurements," Opt. Express **24**(10), 10188–10204 (2016).

#328349 https://doi.org/10.1364/OE.26.016505
Journal © 2018 Received 13 Apr 2018; revised 28 May 2018; accepted 7 Jun 2018; published 13 Jun 2018

Optics EXPRESS

7. R. Ruiz-Lombera, J. Urricelqui, M. Sagues, J. Mirapeix, J. M. López-Higuera, and A. Loayssa, "Overcoming nonlocal effects and Brillouin threshold limitations in Brillouin optical time-domain sensors," IEEE Photonics J. **7**(6), 1–9 (2015).
8. F. Rodriguez-Barrios, S. Martin-Lopez, A. Carrasco-Sanz, P. Corredera, J. D. Ania-Castanon, L. Thévenaz, and M. Gonzalez-Herraez, "Distributed Brillouin Fiber Sensor Assisted by First-Order Raman Amplification," J. Lightwave Technol. **28**(15), 2162–2172 (2010).
9. S. Martin-Lopez, M. Alcon-Camas, F. Rodriguez, P. Corredera, J. D. Ania-Castañon, L. Thévenaz, and M. Gonzalez-Herraez, "Brillouin optical time-domain analysis assisted by second-order Raman amplification," Opt. Express **18**(18), 18769–18778 (2010).
10. Y. Dong, L. Chen, and X. Bao, "Time-division multiplexing-based BOTDA over 100 km sensing length," Opt. Lett. **36**(2), 277–279 (2011).
11. X. H. Jia, Y. J. Rao, C. X. Yuan, J. Li, X. D. Yan, Z. N. Wang, W. L. Zhang, H. Wu, Y. Y. Zhu, and F. Peng, "Hybrid distributed Raman amplification combining random fiber laser based 2nd-order and low-noise LD based 1st-order pumping," Opt. Express **21**(21), 24611–24619 (2013).
12. M. A. Soto, A. L. Ricchiuti, L. Zhang, D. Barrera, S. Sales, and L. Thévenaz, "Time and frequency pump-probe multiplexing to enhance the signal response of Brillouin optical time-domain analyzers," Opt. Express **22**(23), 28584–28595 (2014).
13. Y. Dong, L. Chen, and X. Bao, "Extending the Sensing Range of Brillouin Optical Time-Domain Analysis Combining Frequency-Division Multiplexing and In-Line EDFAs," J. Lightwave Technol. **30**(8), 1161–1167 (2012).
14. M. A. Soto, G. Bolognini, F. D. Pasquale, and L. Thévenaz, "Long-range Brillouin optical time-domain analysis sensor employing pulse coding techniques," Meas. Sci. Technol. **21**(9), 094024 (2010).
15. M. A. Soto, G. Bolognini, F. Di Pasquale, and L. Thévenaz, "Simplex-coded BOTDA fiber sensor with 1 m spatial resolution over a 50 km range," Opt. Lett. **35**(2), 259–261 (2010).
16. M. A. Soto, G. Bolognini, and F. Di Pasquale, "Analysis of pulse modulation format in coded BOTDA sensors," Opt. Express **18**(14), 14878–14892 (2010).
17. M. A. Soto, G. Bolognini, and F. Di Pasquale, "Long-range simplex-coded BOTDA sensor over 120 km distance employing optical preamplification," Opt. Lett. **36**(2), 232–234 (2011).
18. S. Le Floch, F. Sauser, M. Llera, M. A. Soto, and L. Thévenaz, "Colour simplex coding for Brillouin distributed sensors," Proc. SPIE **8794**, *Fifth European Workshop on Optical Fibre Sensors (EWOFS)*, 879437 (2013).
19. S. L. Floch, F. Sauser, M. Llera, and E. Rochat, "Novel Brillouin Optical Time-Domain Analyzer for Extreme Sensing Range Using High-Power Flat Frequency-Coded Pump Pulses," J. Lightwave Technol. **33**(12), 2623–2627 (2015).
20. M. A. Soto, S. Le Floch, and L. Thévenaz, "Bipolar optical pulse coding for performance enhancement in BOTDA sensors," Opt. Express **21**(14), 16390–16397 (2013).
21. Z. Yang, M. A. Soto, and L. Thévenaz, "Increasing robustness of bipolar pulse coding in Brillouin distributed fiber sensors," Opt. Express **24**(1), 586–597 (2016).
22. J. Urricelqui, M. Sagues, and A. Loayssa, "Brillouin optical time-domain analysis sensor assisted by Brillouin distributed amplification of pump pulses," Opt. Express **23**(23), 30448–30458 (2015).
23. X. Hong, W. Lin, Z. Yang, S. Wang, and J. Wu, "Brillouin optical time-domain analyzer based on orthogonally-polarized four-tone probe wave," Opt. Express **24**(18), 21046–21058 (2016).
24. M. A. Soto, J. A. Ramírez, and L. Thévenaz, "Intensifying the response of distributed optical fibre sensors using 2D and 3D image restoration," Nat. Commun. **7**, 10870 (2016).
25. W. Lin, Z. Yang, X. Hong, S. Wang, and J. Wu, "Brillouin gain bandwidth reduction in Brillouin optical time domain analyzers," Opt. Express **25**(7), 7604–7615 (2017).
26. G. Bolognini, J. Park, M. A. Soto, N. Park, and F. Di Pasquale, "Analysis of distributed temperature sensing based on Raman scattering using OTDR coding and discrete Raman amplification," Meas. Sci. Technol. **18**(10), 3211–3218 (2007).
27. J. B. Rosolem, F. R. Bassan, D. E. de Freitas, and F. C. Salgado, "Raman DTS Based on OTDR Improved by Using Gain-Controlled EDFA and Pre-Shaped Simplex Code," IEEE Sens. J. **17**(11), 3346–3353 (2017).
28. F. Wang, C. Zhu, C. Cao, and X. Zhang, "Enhancing the performance of BOTDR based on the combination of FFT technique and complementary coding," Opt. Express **25**(4), 3504–3513 (2017).
29. H. Iribas, A. Loayssa, F. Sauser, M. Llera, and S. Le Floch, "Cyclic coding for Brillouin optical time-domain analyzers using probe dithering," Opt. Express **25**(8), 8787–8800 (2017).
30. M. D. Jones, "Using simplex codes to improve OTDR sensitivity," IEEE Photonics Technol. Lett. **5**(7), 822–824 (1993).
31. D. Lee, H. Yoon, P. Kim, J. Park, and N. Park, "Optimization of SNR Improvement in the Noncoherent OTDR Based on Simplex Codes," J. Lightwave Technol. **24**(1), 322–328 (2006).
32. M. A. Soto, M. Tur, A. Lopez-Gil, M. Gonzalez-Herraez, and L. Thévenaz, "Polarisation pulling in Brillouin optical time-domain analysers," Proc. SPIE **10323**, 103239L (2017).
33. L. Thévenaz, S. F. Mafang, and J. Lin, "Effect of pulse depletion in a Brillouin optical time-domain analysis system," Opt. Express **21**(12), 14017–14035 (2013).

Optics EXPRESS

1. Introduction

During the last decades distributed optical fiber sensing based on Brillouin optical time-domain analysis (BOTDA) [1] has become a mature technology to measure distributed temperature and strain profiles over long optical fibers. The technique is based on the stimulated Brillouin interaction (SBS) between an interrogating optical pulse (so called *pump pulse*) and a counter-propagating continuous-wave (CW) *probe* signal, which occurs when the pump-probe frequency offset falls within the Brillouin gain spectrum (BGS) of the sensing fiber [1,2]. One of the critical parameters defining the performance of a BOTDA system is the signal-to-noise ratio (SNR) of the measurement, and therefore any effort to improve the SNR can lead to a better performing system [2]. However, for a given spatial resolution, the SNR level in a standard BOTDA scheme is proportional to the input pump and probe powers, which are both ultimately limited by nonlinear effects in the sensing fiber. In optimized condition, the maximum tolerable pump power imposed by modulation instability (MI) is ~100 mW in fibers longer than 20 km [3,4], while the probe power is limited to −6 dBm per sideband in a conventional dual-sideband configuration to mitigate the impact of higher-order nonlocal effects [5–7].

To further enhance the SNR beyond the conventional single-pulse BOTDA, several advanced techniques have been proposed during the last decade [6–25]. As one of the most efficient approaches, *optical pulse coding* has been extensively developed [14–21]. In this technique, series of coded optical pulse sequences are launched into the sensing fiber, thus increasing the pump energy while keeping the peak power of each pulse strictly limited below MI threshold. After a decoding process, the single-pulse BOTDA response can be retrieved with enhanced SNR, and the spatial resolution is maintained as determined by the width of each pulse in the code sequence [14–17]. Plenty of coding schemes have been demonstrated, such as unipolar unicolor codes (with 0's and 1's code elements), time-frequency codes (also called colored) [18,19] and bipolar codes (with −1's and 1's elements) [20,21]. In all these cases, the SNR enhancement is determined by the so-called *coding gain*, which is typically proportional to the square-root of the code length [14–21].

However, in early stages of the coding implementation [14–17] (and not only in Brillouin-based sensor [26]), boosting the peak power of the coded optical pump sequences using lumped optical amplification, e.g., using erbium-doped fiber amplifier (EDFA), was identified as one of the most challenging issues to preserve the linearity of the code, since the slow gain recovery of the amplifier typically leads to unevenly-amplified pulses within the code sequence [14]. In such a condition (without EDFA), the maximum power of the pump coded sequences was generally limited by the maximum output power of electro-optic modulators (being typically ~15 dBm at the input of the sensing fiber), which is far lower than the optimal power limit imposed by MI (~100 mW, as found years later [3,4]). For this reason, the capabilities and limitations of pulse coding have been essentially investigated under sub-optimal conditions, although the theoretical coding gain can be clearly verified in experiments when comparing with a single-pulse BOTDA scheme that uses the same sub-optimal pulse peak power. Recently, sophisticated solutions have been proposed in the literature to make a flat coded sequence amplification [26–29], enabling optimizing the power of coded sequences. This progress offers the opportunity to fully evaluate the fundamental limitations and real benefits of coded BOTDA schemes and compare them with a fully optimized standard single-pulse BOTDA system. More recently, it has been indeed found out that the high Brillouin amplification resulting from unipolar coding can induce distortions in the decoded traces, while higher-order nonlocal effects can be very detrimental [29]. However, a quantified evaluation of the real impact of the pump and probe powers on the overall performance of the sensor, along with a design tool to fully optimize the performance of unipolar unicolor coded BOTDA system, is still missing in the literature.

Optics EXPRESS

In this paper the fundamentals of unipolar unicolor coded BOTDA are investigated and revisited, along with a thorough analysis regarding the impact of the large accumulated Brillouin amplification on the sensor performance. In this work, conventional unipolar Simplex and Golay coding techniques are both considered for systems targeting meter-scale spatial resolutions and long sensing distances (>25 km), for which pulse coding primarily makes sense. First, the study focuses on investigating the detrimental impact of conventional linear normalization process, such as decoded-trace distortions and systematical BFS estimation errors, in case of large accumulated Brillouin amplification. A solution based on logarithmic normalization is then proposed, which is theoretically and experimentally validated as a robust approach to retrieve the accumulated Brillouin gain without any approximation. Then, the paper analyzes the impact of an imperfect power equalization between the pulses of the code sequences, polarization pulling effects and higher-order nonlocal effects associated to a cascaded pump depletion phenomenon. Results point out that Golay codes are highly sensitive to pulse peak power variations, and can lead to significant distortions. This effect is however averaged out in the case of Simplex codes. On the other hand, the analysis on polarization pulling shows that, contrarily to single-pulse BOTDA, significant changes in the state of polarization of the probe signal can occur due to the strong Brillouin interaction cumulated over the code sequences. While large uncompensated polarization fading can remain on the decoded traces if a polarization switch is used, these detrimental fading can be highly mitigated using a polarization scrambler. After optimizing all conditions for a proper operation of unipolar pulse coding, the limitations imposed by higher-order nonlocal effects are thoroughly analyzed. Results indicate that a cascaded depletion effect occurs over the different pulses of the coded sequence, imposing limitations to the maximum probe power that can be launched into the sensing fiber. The impact of this probe power limitation on the overall SNR improvement provided by coding, when compared to a fully optimized single-pulse BOTDA scheme, is modelled and experimentally verified.

2. Traditional unipolar pulse coding in BOTDA sensors: General concepts

A common and most straightforward way to implement a coded BOTDA system is to use unipolar unicolor codes based on either Simplex or Golay codes, containing coded elements (bits) being '0s' and '1s' [14–17]. Let M represents the code length and N denotes the number of '1' elements, in both Golay and Simplex codes N is close to $M/2$ (as a first-order approximation). The structure of the codes is typically defined by a 'coding matrix', whose dimension is $M \times M$ or $4 \times M$ for Simplex or Golay codes. Defining the temporal width of each pulse in the code sequence as W, the spatial resolution is given as $\Delta z = v_g W/2$, where v_g is the group velocity in the sensing fiber. In order to mitigate the Brillouin cross interaction between two adjacent coding symbols imposed by the inertial feature of the acoustic wave, a return-to-zero (RZ) pulse coding format must be utilized [16]. The duration of each RZ code bit (including the pulse width and the section at zero level) is denoted as T_d, as shown in Fig. 1, in which the time duration of the zero level T_d -W must be a few times longer than the acoustic response time (~10 ns). Consequently, the temporal duration of the overall code sequence is $T_c = T_d M$, as illustrated in Fig. 1.

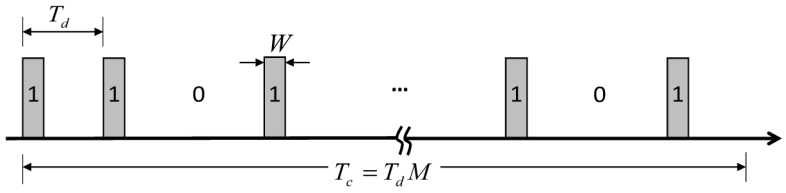

Fig. 1. Illustration of an RZ coded sequence '1101…101' with M coding units

Optics EXPRESS

Along the sensing fiber, each coded pump pulse interacts with a counter-propagating probe wave through SBS at different fiber positions, leading to an accumulated Brillouin amplification/depletion on the lower/higher frequency probe component. The theoretical description of this process is presented here below, by assuming a Brillouin gain configuration in which the optical frequency of the interacting probe is lower than the optical frequency of the coded pump. At a given arbitrary time $t \geq T_c$ after the first pulse of the coded sequence entering the fiber, the Brillouin interaction takes place at different fiber positions over a fiber section ranging from z - L_c to z, where $z = v_g t$ is the position of the first pulse of the sequence and $L_c = T_c v_g$ is the fiber section covered by the code. For the sake of clarity, the fiber loss experienced by both pump and probe waves, over the fiber section L_c covered by the code (typically a few kilometers), is here neglected. Note that this assumption is not always required for all kind of codes, but makes the analysis presented hereafter valid for a broader range of code types. Under this generally-valid assumption, the intensity of the probe wave after experiencing the SBS interaction can be expressed as:

$$P_S(z-L_c,\nu) = P_S(z)\underbrace{\exp\left[g_{s\_1}(z,\nu)\right]\exp\left[g_{s\_2}(z-L_d,\nu)\right]\cdots\exp\left[g_{s\_3}(z-(M-1)L_d,\nu)\right]}_{Cascaded\ gain}$$
$$= P_{iS}\exp\left[-\alpha(L-z)\right]\exp\left[\sum_{i=1}^{M} g_{s\_i}(z_i,\nu)\right] \quad (1)$$

where P_{iS} is the input probe power at $z = L$, ν is frequency detuning, z_i is equal to z-(i-1)L_d, corresponding to the fiber position where the i^{th} coded pulse interacts with the probe, and g_{s_i} is the linear Brillouin amplification provided by the i^{th} coded pulse, which can be represented as:

$$g_{s\_i}(z_i,\nu) = \begin{cases} g_B(z_i,\nu)P_{iP}\exp(-\alpha z)\Delta z & \text{for} \quad C_i = 1 \\ 0 & \text{for} \quad C_i = 0 \end{cases} \quad (2)$$

where $g_B(z_i, \nu)$ is the local Brillouin gain coefficient at a frequency detuning ν, Δz is the spatial resolution, P_{iP} represents the peak power of the injected coding sequence at the input of the fiber (z = 0), and C_i denotes the state of the i^{th} coded pulse being either 0 or 1 in the case of unicolor unipolar codes, (e.g., Golay or Simplex codes). Assuming that the BFS profile over the fiber section spanning from z - L_c to z is uniform, corresponding to the worst case in term of cumulated amplification, the contribution of each '1' in the coding sequence can be considered identical, so that Eq. (1) can be re-written as:

$$P_S(z-L_c,\nu) = P_{iS}\exp\left[-\alpha(L-z)\right]\exp\left[G(z,\nu)\right] \quad (3)$$

where $G(z,\nu)$ represents the cumulated linear Brillouin amplification:

$$G(z,\nu) = \frac{M}{2}g_s(z,\nu) = \frac{M}{2}g_B(z,\nu)P_{iP}\exp(-\alpha z)\Delta z \quad (4)$$

where $g_s(z, \nu)$ stands for Brillouin amplification attributed to each coding pulse (i.e., single-pulse Brillouin gain). After interacting with the code sequence at position z, the local probe wave described by Eq. (3) continues its propagation over the fiber, in the absence of SBS interaction, until being detected at the sensing fiber input z = 0. Thus, the amplified probe in Eq. (3) just experiences the natural fiber loss from the interaction point z to the fiber input z = 0, resulting in a measured probe wave given by:

Optics EXPRESS

$$P_S^0(z,\nu) = P_S(z-L_c,\nu)\exp(-\alpha z) = P_{iS}\exp(-\alpha L)\exp\left[G(z,\nu)\right] \quad (5)$$

The measured coded BOTDA trace, as depicted in the left frame of Fig. 2, is composed of the cumulated SBS amplification given by the coded pulse sequence, together with a DC component corresponding to the CW probe reaching the fiber near end without Brillouin amplification. This DC component can be simply expressed by removing the Brillouin gain term from Eq. (5):

$$P_S^{0\_DC} = P_{iS}\exp(-\alpha L) \quad (6)$$

Since traditional (linear) coding techniques require the linear superposition of the BOTDA traces contributed from all the code pulses, the accumulated linear Brillouin amplification $G(z,\nu)$ must be extracted from the raw measured data through a normalization process, as illustrated by the central frame in Fig. 2. After calculating the accumulated Brillouin amplification, the linear amplification $g_s(z, \nu)$ associated to a single pulse (see the right frame depicted in Fig. 2) can be retrieved by a dedicated decoding process. Note that $G(z,\nu)$ may be a few hundred times larger than $g_s(z, \nu)$, leading to more significant nonlinear distortions with respect to a traditional single-pulse BOTDA, which may give rise to a detrimental impact on the sensing performance. In the following sections, the relevant phenomena along with the corresponding solutions and optimization process in the case of unipolar unicolor coded BOTDA will be thoroughly studied and demonstrated.

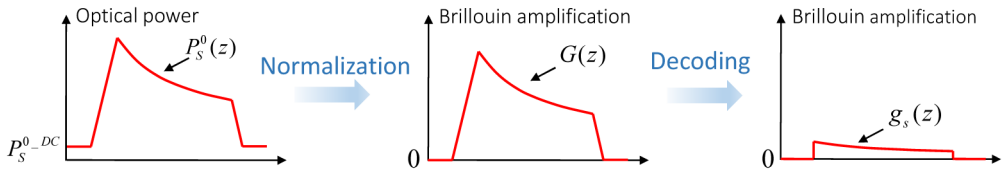

Fig. 2. Schematic illustration of general decoding process for a given ν.

3. Experimental setup

The experimental setup for this study is shown in Fig. 3. The light from a distributed feedback laser (laser1) is split into pump and probe branches using an optical coupler. In the probe branch (upper arm in the figure), the continuous-wave light is injected into a high extinction ratio (40 dB) electro-optic modulator (EOM1), operating at null transmission point to generate a carrier-suppressed double-sideband (CS-DSB) wave, using a tuneable RF signal that scans over the BGS of the sensing fiber. A polarization switch (PSw) is then connected to minimize the impact of polarization on the Brillouin gain, followed by a circulator that allows the probe light to be launched into the sensing fiber while monitoring the optical power of the coded sequence (launched through the opposite end of the fiber) at the output of the sensing fiber.

Optics EXPRESS

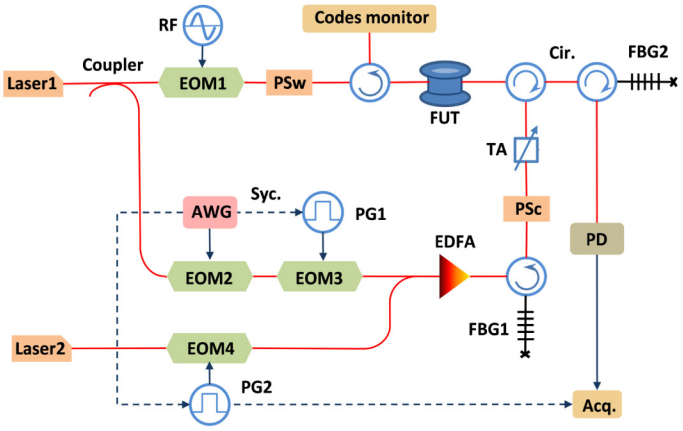

Fig. 3. Experimental setup.

In the pump branch (lower arm in the figure), the light is modulated in intensity by using an electro-optic modulator (EOM2) driven by an arbitrary waveform generator (AWG) with 2 GSa/s sampling rate delivering an RZ pulse sequence with code length of M bits. The width of each pulse is set as 20 ns, corresponding to a spatial resolution of 2 m and a duty cycle of 16.7% in return-to-zero format (T_d = 120 ns). In order to obtain a coded pump with high extinction ratio, the optical pulse sequence is further gated by EOM3 driven by a long electrical pulse of width $T_c = T_d M$ generated by a pulse generator (PG1). To alleviate the well-known uneven power amplification of the coded pulses resulting from transient effects within the EDFA [14], an additional optical pulse at a different wavelength (from laser2) is launched in front of the coded pulse sequence to saturate the EDFA. By properly adjusting the power, the extinction ratio and the width of this additional optical pulse, the flatness of the coded pulse sequence can be highly improved [28]. This additional pulse is then filtered out by a fiber Bragg grating (FBG1) after the EDFA, so that only the coded pulse sequence is launched into the sensing fiber after passing through a polarization scrambler (Psc) and a tunable attenuator (TA). Note that either the PSw or the PSc is used for the measurements, allowing for a suitable comparison of the impact of the used polarization diversity scheme (e.g., eventual polarization pulling effects, as it will be discussed in Section. 6).

At the receiver, an FBG (FBG2) with 6 GHz filtering bandwidth is placed before the photodetector to select either the lower or higher frequency probe sideband for either Brillouin gain or loss configuration.

4. Impact of normalization procedures on the sensing performance

4.1 Conventional linear normalization

As previously described, an important intermediate step with coded BOTDA is to extract the linear Brillouin amplification $G(z,\nu)$ from the detected raw signal represented by Eqs. (5) and (6). This is generally realized by using conventional linear normalization expressed as:

$$G(z,\nu) \approx \frac{P_S^0(z,\nu) - P_S^{0\_DC}}{P_S^{0\_DC}} = \exp\left[G(z,\nu)\right] - 1 \qquad (7)$$

provided that $G(z,\nu)$ is far smaller than 1. This small gain condition can be absolutely secured in a single-pulse BOTDA (i.e., N = 1), in which the maximum Brillouin gain is in the order of 1% (assuming an optimized peak pump power of ~100 mW, as imposed by MI). In addition, this small gain assumption is also satisfied in some implementations of unipolar coded BOTDA reported in the literature [14–17], which have used either low peak pulse powers or a reduced number of bits to ensure a low $G(z,\nu)$ level. However, in these implementations the

Optics EXPRESS

overall SNR performance is therefore compromised when compared to a fully optimized system.

When an optimal peak power and long code sequences are simultaneously used, the $G(z,\nu)$ at the fiber input and at the resonance peak frequency, denoted as G_0, can reach and even be larger than 200% (e.g., 100 mW peak power and 512 bits code length), thereby violating the above mentioned small-gain condition. Consequently, the nonlinear contribution of the exponential term in Eq. (7) becomes non-negligible, giving rise to errors on the $G(z,\nu)$ extracted from conventional linear normalization process, and inducing distortions in the decoded local Brillouin gain distribution [29]. To illustrate the impact of this nonlinear Brillouin interaction, experiments employing unipolar unicolor Golay and Simplex coding are both carried out using a 47 km-long sensing fiber. The pulse peak power is set to ~100 mW and each pulse width is 20 ns (2 m spatial resolution), leading to a $g_s(z,\nu)$ of ~1% at the beginning of the sensing fiber and at the peak resonance frequency. The code length M is adjusted to be 128, 256 and 512 bits for Golay coding, and 127, 255 and 511 bits for Simplex coding, resulting in G_0 levels varying as 60%, 120% and 240%, respectively. In order to mitigate the impact of higher-order nonlocal effects, the probe power per sideband is deliberately adjusted to −17 dBm (details for this choice will be discussed in Section 7). Note that in this case the polarization scrambler placed on the pump branch is used to minimize polarization fading in the BOTDA traces, while the polarization switch on the probe branch is turned off.

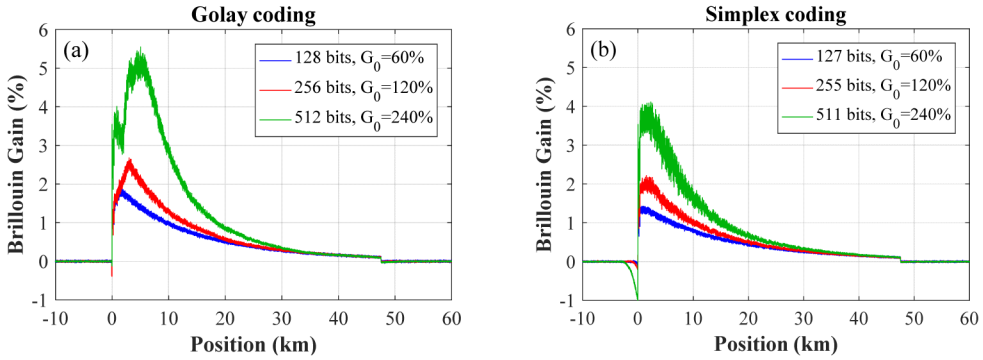

Fig. 4. Decoded Brillouin gain traces after conventional linear normalization for different G_0, using (a) Golay and (b) Simplex codes.

Figures 4(a) and 4(b) show the decoded z-dependent $g_s(z,\nu)$ distributions at the resonance peak frequency, when employing traditional linear normalization process along with Golay and Simplex coding, respectively. Note that none of the decoded traces agrees with the expected g_s value of 1% at the fiber input. Furthermore, clear trace amplitude distortions are observed, while the level of distortion depends on the accumulated (nonlinear) SBS amplification, i.e., $\exp[G(z,\nu)]$, in the coded BOTDA traces. To reduce these Brillouin-gain-dependent distortions, $G(z,\nu)$ must be restricted if using conventional linear normalization, which imposes a fundamental limit to the allowable code length, consequently impacting on the overall SNR and BOTDA performance.

4.2 Proposed solution: logarithmic normalization

Indeed, the exponential behavior of the overall Brillouin gain on the probe signal of a BOTDA sensor makes more appropriate the use of a logarithmic normalization for retrieving the linear Brillouin amplification $G(z,\nu)$, which can be mathematically expressed as:

$$G(z,\nu) = \ln\left[\frac{P_S^0(z,\nu)}{P_S^{0\_DC}}\right] \tag{8}$$

Optics EXPRESS

It must be mentioned that although the main motivation to use this newly proposed logarithmic normalization is to extract $G(z,v)$ in an optimized coded-BOTDA system, this normalization is indeed also valid for any level of Brillouin amplification, including both small and large gain regimes, so being totally universal.

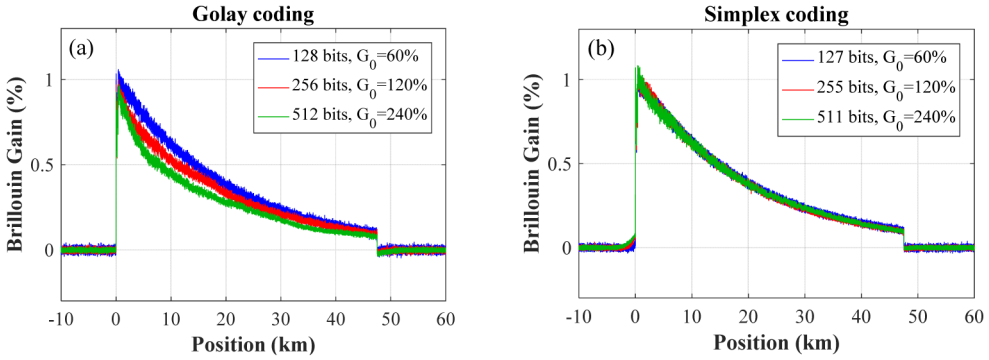

Fig. 5. Decoded Brillouin gain traces after the proposed logarithmic normalization for different G_0, using (a) Golay and (b) Simplex codes.

To demonstrate the feasibility of this proposal, the same experimental raw data used for retrieving the curves in Figs. 4(a) and 4(b) under linear normalization are re-used here exploiting the logarithmic normalization. The resulting decoded curves for both Golay and Simplex coding techniques are illustrated in Figs. 5(a) and 5(b), respectively, showing a good match with the expected Brillouin gain (1% at the beginning of the fiber) for all the curves. Furthermore, it appears clearly that none of the curves shows nonlinear-gain induced distortions. Indeed the three decoded curves exhibits exactly the same trend when using Simplex coding (Fig. 5(b)) regardless of $G(z,v)$, demonstrating the beneficial improvement provided by the logarithmic normalization. However, it should be noticed that in the case of Golay coding the decaying trend is different under different gain values, as shown in Fig. 5(a). As the length of Golay code sequences increases, the decoded curve exhibits a larger amplitude shortfall with respect to a standard exponential decay. The reason of such a behavior actually comes from the power non-uniformity of the coded pump pulses after amplification through EDFA, which is very detrimental for Golay coding performance, as it will be further discussed in Section 5.

Optics EXPRESS

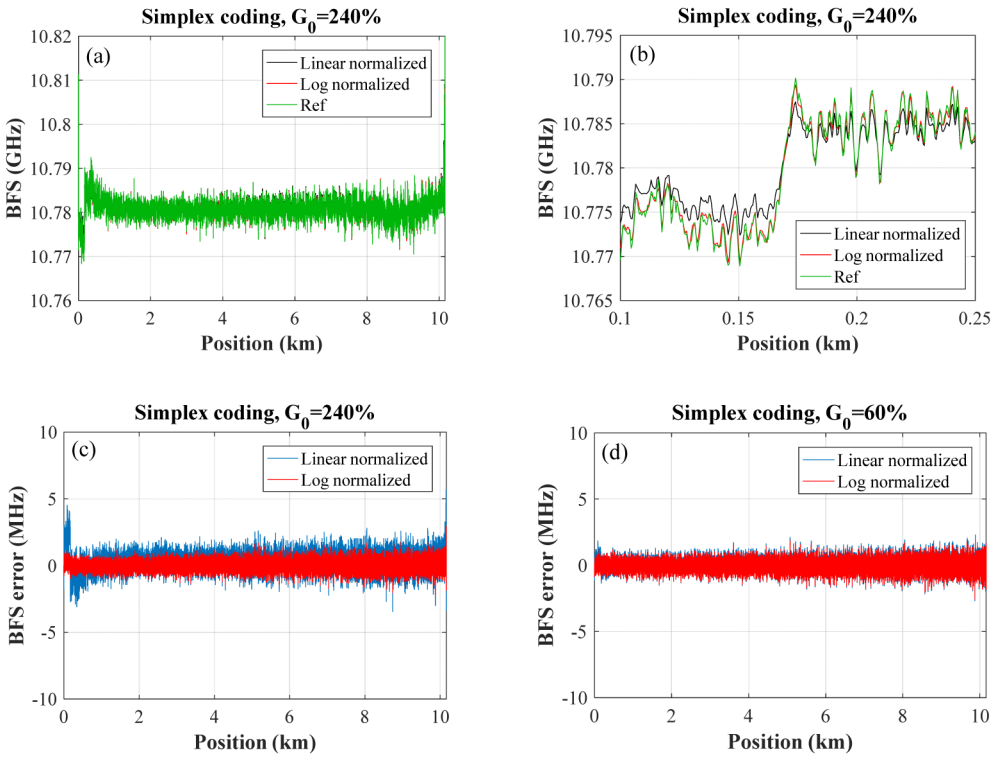

Fig. 6. (a) BFS profiles over the whole sensing fiber, obtained from a single-pulse BOTDA and a Simplex coded BOTDA with different normalization methods in case of G_0 = 240%. (b) BFS profiles over a fiber section from 100 m to 250 m. (c) BFS error profiles over the sensing fiber in case of G_0 = 240%. (d) BFS error profiles over the sensing fiber in case of G_0 = 60%.

In order to compare the impact of the conventional linear normalization and the proposed logarithmic normalization on the retrieved BFS profile, a full BOTDA frequency scan has been performed using both Golay and Simplex coding. Since the fiber length is not relevant in this study, and for the sake of visual clarity (i.e., to have a high SNR), a relatively short (10 km-long) SMF with non-uniform BFS distribution (varying over 15 MHz) is deliberately used. The BOTDA configuration is similar to that used in Section 4.1, and the final BFS profile is obtained following the decoding procedure depicted in Fig. 2 associated with a quadratic fitting process applied on each local BGS [2]. The results obtained using Simplex coding with 511 bits coding length, which corresponds to a large G_0 of 240%, are shown in Fig. 6(a), where the black and red curves represent the BFS profiles resulting from linear and logarithmic normalizations, respectively. A reference BFS profile (green curve) taken by standard single-pulse BOTDA is also provided for comparison. From Fig. 6(a) it is hard to observe significant differences among these three curves; however, clear deviations can be seen in Fig. 6(b), which shows the BFS profile of the fiber section spanning from 100 m to 250 m, where a sharp BFS transition region is located at ~170 m. Results demonstrate that the BFS profile obtained from logarithmic normalization is in good agreement with the reference, while the one resulting from linear normalization shows clear frequency deviations that can reach up to a few MHz. In order to better evaluate the BFS errors induced by the normalization process, the reference BFS profile (green curve in Fig. 6(a)) is subtracted from the red and black curves, as shown in Fig. 6(c). One can observe that the BFS error resulting from logarithmic normalization is always below 1 MHz, which is actually dominated by the detection noise. However, the linear normalization results in non-negligible BFS errors all along the fiber, which can reach up to 4 MHz nearby the transition region. These results

Optics EXPRESS

validate the necessity of using the proposed logarithmic normalization method in high Brillouin gain regime. Reducing G_0 from 240% down to 60% by changing the code length from 512 bits to 128 bits, the BFS error can be greatly alleviated in the case of linear normalization, as it can be observed comparing Fig. 6(c) and Fig. 6(d). However, it should be noted that in this case the SNR improvement brought by the coding technique is thereby reduced accordingly due to the shorter code length.

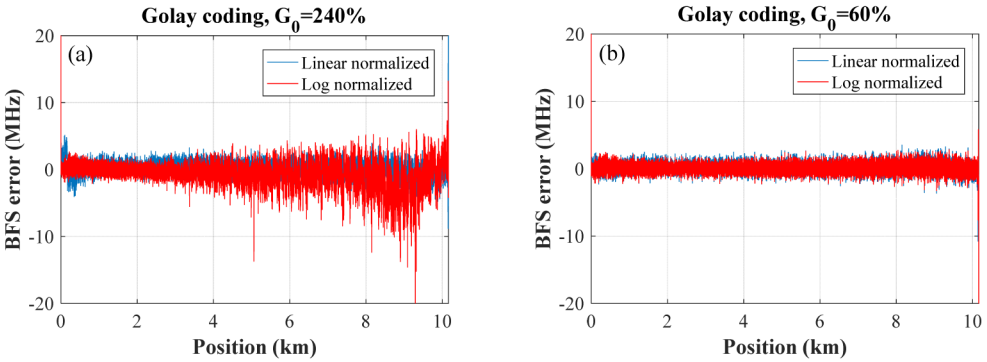

Fig. 7. BFS error profiles over the sensing fiber in case of Golay coding when (a) G_0 = 240% and (b) G_0 = 60%.

A similar comparison has also been carried out using Golay coding. Figure 7(a) and (b) show the BFS error profiles in cases of G_0 = 240% and G_0 = 60%, respectively. In contrast with Simplex coding, the logarithmic normalization does not result in negligible errors when G_0 = 240%. Indeed, part of this BFS distortion originates from the power non-uniformity of the amplified coded pump pulses, which is linked to the decoded BOTDA trace distortion (green curve) in Fig. 5(a), and will be analyzed in detail in Section 5. When the code length is reduced down to 128 bits, this detrimental artefact is mitigated, as shown by the blue curve in Fig. 5(a), thus resulting in negligible BFS errors (as shown in Fig. 7(b)), which are essentially dominated by detection noise.

5. Power non-uniformity of the coded optical pulses

As mentioned in Section 3, an additional optical pulse (generated by laser2 and EOM4 in Fig. 2) has been utilized before sending the code sequence into the EDFA to reduce the population inversion of the amplifier, thus enabling code sequences with relatively uniform and high peak pulse power after amplification. However, in this section we point out that even with this solution, the power of amplified coding pulses still exhibit slight non-uniformity, which may impact negatively on the coding performance. This power non-uniformity is due to the specific distributions of '1's and '0's on the different code sequences (for both unipolar Golay and Simplex codes). The power level of each pulse indeed depends on the time separation between coded pulses. The longer the separation between two consecutive '1' code symbols, the more time left for rebuilding the population inversion in the EDFA, and thus the larger the amplification of the latter code symbol. These slightly distinct amplification levels for the different coded pulses may break the linearity of the code, deteriorating the performance of coding techniques. Note that this effect highly depends on the properties of the code, therefore different behaviors are expected for Golay and Simplex codes.

In order to evaluate the impact of the power non-uniformity between pulses in Golay codes, the four unipolar Golay coded pulse sequences (denoted as A1, A2, B1 and B2) with uniform amplitude are measured before entering the EDFA as references, which are sequentially plotted in Fig. 8(a), where the coding length has been set to 512 bits. As above explained, after EDFA amplification, even though the pre-depletion pulse is already

Optics EXPRESS

optimized for the first Golay coded sequence A1, each pulse sequence presents specific and reproducible optical power distributions, as illustrated in Fig. 8(b).

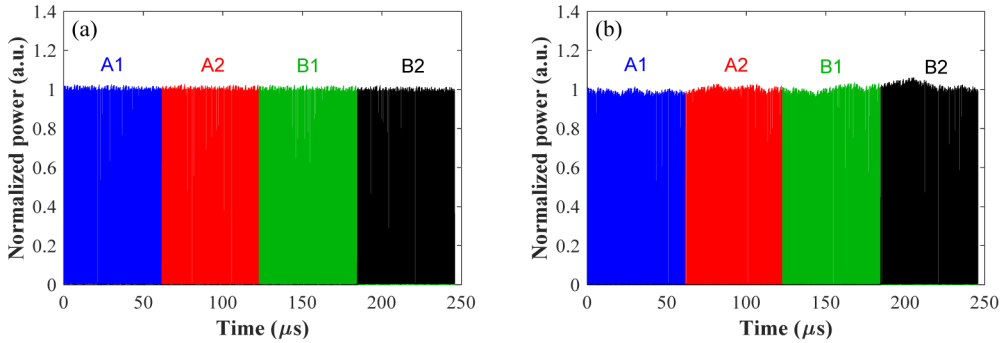

Fig. 8. Impact of EDFA amplification on code sequence amplitude. Normalized 512-bit Golay coded optical pulse sequence (a) at the EDFA input and (b) at the EDFA output.

The decoding process of Golay codes relies on the autocorrelation properties of complementary coded sequences, therefore any perturbation on the amplitude of the original Golay codes could potentially impact on the decoding performance. To investigate this, the sum of the autocorrelation functions of the pulse sequences before and after EDFA (curves in Fig. 8(a) and (b)) are carried out, respectively. Figure 9(a) shows the result attributed to the coded sequences before EDFA, which consists of a main correlation peak and small residual sidelobes originating essentially from the noise in the measured pulse sequences. A worse behavior can be found when using the coded sequences after EDFA, as illustrated in Fig. 9(b), since sidelobes with larger amplitude appear in the autocorrelation function. These residual correlation sidelobes carry the Brillouin gain/loss information from their corresponding positions (i.e., from the entire fiber section covered by the autocorrelation function), contaminating the local gain/loss information that should only be attributed to the main correlation peak. This peculiarity is indeed similar to the effect existing in unbalanced bipolar Golay codes reported in [21]. The detrimental impact resulted from the additional sidelobes can also be indicated in Fig. 7(a), in which the BFS profile obtained after Golay coding/decoding shows significant errors even though the logarithmic normalization is used. Therefore, it is important to secure that the integrated amplitude confined in the residual sidelobes is much smaller (e.g., < 10%) than the one in the main correlation peak. Using the data shown in Fig. 9 and integrating the contribution of the main correlation peak and the residual sidelobes, it turns out that in the case of a flat coded sequence (before EDFA), the total contribution of the sidelobes is just 4% (with positive sign), while in the case of uneven coded sequences, the contribution of the sidelobes reaches 36% (with negative sign) with respect to the main correlation peak. This effect is also confirmed by the green curve shown in Fig. 5(a), which shows a gain reduction of 36% at all fiber positions where the entire code sequence is located inside the fiber. Experiments are performed by reducing the code length from 512 bits to 256 bits and further down to 128 bits; the contribution of the negative sidelobes is calculated to be reduced down to 17% and 7% with respect to the main correlation peak, respectively. This is also in good agreement with the red and blue curves shown in Fig. 5(a), confirming the negligible levels of BFS errors shown in Fig. 7(b) when 128-bit Golay codes are used.

Optics EXPRESS

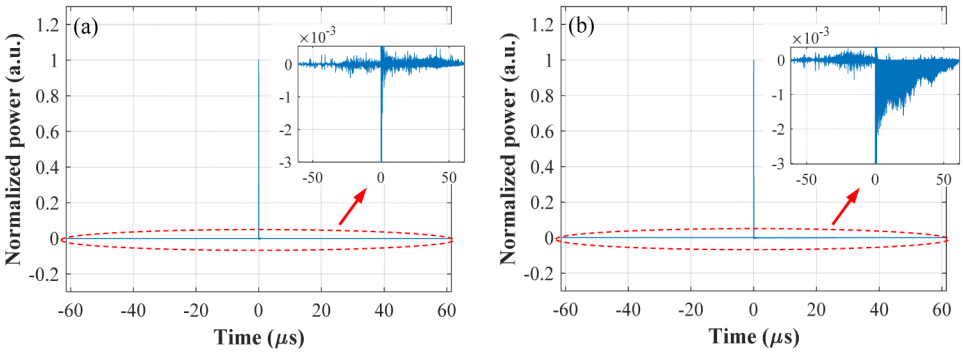

Fig. 9. Decoded autocorrelation functions using the coded sequences with 512-bit coding length measured (a) at the EDFA input and (b) at the EDFA output.

Note that the level of distortion in the decoded traces is mainly related to the code length, but has no clear relation with the pulse peak power. To verify this, experiments are carried out with the same G_0 levels as in Fig. 5, by adjusting the pulse peak power while maintaining a code length of 512 bits. The decoded traces, shown in Fig. 10, exhibit in all cases large levels of distortion, even when G_0 is reduced down to 60%.

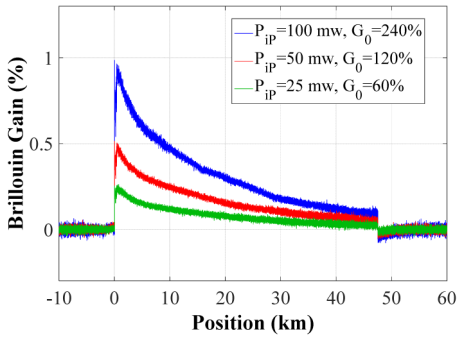

Fig. 10. Decoded Brillouin gain traces after logarithmic normalization for different G_0 levels using 512-bit Golay coded BOTDA.

In the case of Simplex coding, the situation is different, since the principle does not depend on the correlation properties of the code sequences. The decoding process for Simplex codes is entirely linear, which is based on a matrix inversion and linear averaging of traces [30,31]. In other words, the decoded Brillouin gain is attributed to the mean value of all the coding pulses, therefore the impact of the pulse power non-uniformity is highly averaged and hence greatly mitigated. This can be visualized in Fig. 5(b), where the decoded traces obtained using Simplex coded BOTDA do not show any visible distortion.

In summary, Golay codes require much stricter conditions than Simplex codes to obtain non-distorted decoded Brillouin gain traces. When the BFS distribution along the fiber is uniform, the negative impact manifests as decoded gain traces with lower amplitude, eventually affecting the SNR performance. However, if the BFS distribution of the fiber is non-uniform, large frequency errors appear in the retrieved BFS profile. The key to overcome this detrimental effect in Golay codes is to make each code symbol to be non-zero in all the coding sequences, which is actually the case when implementing bipolar Golay codes [20,21], where pump pulses at either Stokes or anti-Stokes frequencies fill each bit position. Due to this strict condition required by Golay codes to operate without introducing distortions, the analysis presented in the following sections of this paper will focus on the more robust

Optics EXPRESS

Simplex coded BOTDA systems, in which the proposed logarithmic normalization can be safely used.

6. Impact of polarization pulling

The impact of polarization pulling has been recently investigated with a standard single-pulse BOTDA scheme, in which the state of polarization (SOP) of the pump pulse is modified during the SBS interaction with the probe wave along the full fiber length, giving rise to uncompensated polarization fading that degrades the SNR of the sensor [32]. Since the maximum probe power allowed in the fiber is limited to about −6 dBm to avoid BGS distortions [5,6], the impact imposed by polarization pulling is typically negligible [32]. However, we find out that in a coded-BOTDA system the polarization pulling is much more significant due to large Brillouin amplification. Note that this situation is very different from a single-pulse BOTDA [32], where the SOP of the pulse is modified by the probe while the probe SOP is marginally affected. Here the cumulated effect of the pump coding sequence makes the SOP of the probe considerably modified, so that uncompensated polarization fading due to pulling predominantly occurs along the first kilometers of fiber. The power within the pumping code sequence is here the highest, offering a favorable situation for polarization pulling. This means that when using a polarization switch, the summation of the Brillouin amplification on the two sequentially launched probe waves with orthogonal SOPs cannot fully compensate the polarization fading. One solution to alleviate this detrimental effect is to make the SOP of each coding pulse fully uncorrelated, using for instance a polarization scrambler ideally on pump branch (to avoid additional noise introduced by the scrambler if placed on the probe branch).

Comparative measurements of either using a polarization switch (on the probe branch) or a polarization scrambler (on the pump branch) have been carried out with a 511-bit Simplex coded BOTDA. The experimental conditions are the same as the one performed in Section 4 using a 47 km-long sensing fiber. The decoded Brillouin gain traces after logarithmic normalization are shown in Fig. 11(a) for the case of G_0 = 240%. It can be found that when using polarization switch, strong residual uncompensated polarization fading appear at the near end of the fiber (blue curve), and as the Brillouin gain reduces along the fiber due to the fiber loss, the polarization fading gradually vanishes. On the contrary, no obvious polarization fading can be observed when using a polarization scrambler (red curve), demonstrating that polarization pulling effects can be greatly minimized by randomizing the SOP of each coded pulse. When G_0 is reduced down to 60%, the presence of uncompensated residual polarization fading is however not evident in any of the two cases, as illustrated in Fig. 11(b).

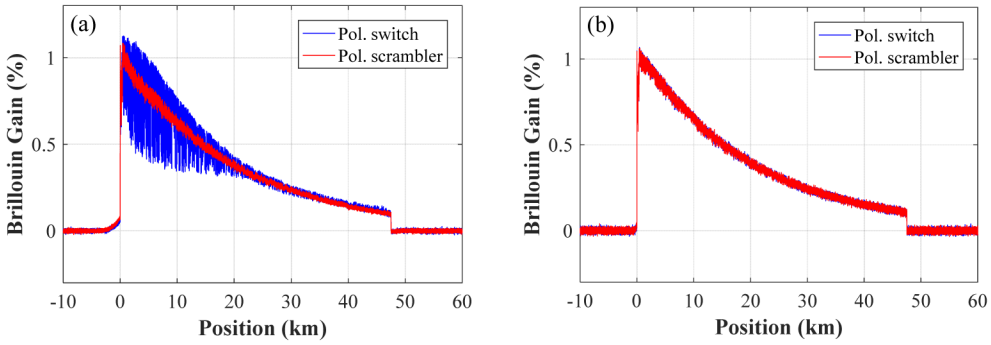

Fig. 11. Decoded Brillouin gain traces after logarithmic normalization (when using polarization switch or polarization scrambler) for the cases of (a) G_0 = 240% and (b) G_0 = 60%.

Optics EXPRESS

7. Higher-order non-local effect

In previous sections, the factors impacting on the SNR performance of unipolar coded-BOTDA systems, such as decoding distortion and polarization pulling effect, are analyzed and overcome by dedicated solutions (logarithmic normalization and the use of polarization scrambler). The remained critical aspect to ultimately optimize the overall SNR is to determine the maximum probe power allowed to be launched into the sensing fiber. It has been reported that in unipolar coded BOTDA systems, higher-order nonlocal effects can easily occur, which may restrict the incident probe power below the maximum probe power (−6 dBm) tolerated in single-pulse BOTDA. Although this effect has been evaluated in [29], the demonstrative experiment has been carried out using conventional linear normalization, which eventually biases the pure impact of higher-order nonlocal effects. Thus, the acceptable level of pump depletion still remains unclear, and for a given depletion level the required probe power has not been quantified yet. Here the proposed logarithmic normalization can completely eliminate the impact of large Brillouin amplification on decoding distortion, allowing for focusing on investigating and optimizing the probe power.

Actually, in single-pulse based BOTDA, the so-called first-order non-local effect has been analytically modelled and quantified [33], and proved to induce systematic errors on the estimated BFS profile, especially at locations close to the far end of the sensing fiber [33]. The higher-order non-local effect is also preliminarily analyzed in [33], under the assumption of a small-gain approximation. This approximation is not valid in unipolar coding technique where much larger Brillouin amplification may appear; therefore a mathematical modelling for more general conditions is needed, in which the power of the lower and upper frequency probe sidebands, i.e., P_{SL} and P_{SU}, must be expressed with no assumptions:

$$P_{SL}(z) = P_{iSL} f_{SL}(z) = P_{iSL} \exp\left[-\alpha(L-z)\right]\exp\left[G(z,\nu)\exp(-\alpha z)\right] \tag{9}$$

$$P_{SU}(z) = P_{iSU} f_{SU}(z) = P_{iSU} \exp\left[-\alpha(L-z)\right]\exp\left[-G(z,\nu)\exp(-\alpha z)\right] \tag{10}$$

where P_{iSL} and P_{iSU} represent the power of the lower and upper frequency sidebands injected at the far fiber end ($z = L$), and $f_{SL}(z)$ and $f_{SU}(z)$ are functions taking into account the exponential behavior of the accumulated Brillouin amplification and fiber attenuation. From Eqs. (9) and (10) it can be observed that large values of $G(z,\nu)$ can easily unbalance the power of the lower and higher frequency sidebands. It is then expected that the n^{th} coded pulse will interact with probe sidebands that have been considerably amplified/depleted by all the previous (from 1 to n-1) pulses of the code sequence. Consequently the n^{th} pulse would experience a higher depletion than the (n-1) previous pulses, and the depletion of the last pulse would be the highest. This cascaded depletion effect can be experimentally verified, as shown in Fig. 12(a), where the power distribution of 511-bit Simplex coded sequences at the output of a 47-km long fiber are illustrated under the conditions that the probe wave is turned on and off.

In order to quantitatively investigate this cascaded pump depletion effect, the depletion level d of the last coding pulse is mathematically evaluated by integrating the power difference between the two probe sidebands (Eqs. (9) and (10)):

$$1-d = \exp\left[-g_B(\nu)\left(\int_0^L P_{SL}(z)dz - \int_0^L P_{SU}(z)dz\right)\right] \tag{11}$$

Since the input powers of the two probe sidebands are equal, i.e., $P_{iSL} = P_{iSU} = P_{iS}$, Eq. (11) can be expressed as a function of $f_{SL}(z)$ and $f_{SU}(z)$ defined in Eq. (9)-(10) as:

$$1-d = \exp\left[-g_B(\nu)P_{iS}\left(\int_0^L f_{SL}(z)dz - \int_0^L f_{SU}(z)dz\right)\right] \tag{12}$$

Optics EXPRESS

which matches well with the experimental results shown in Fig. 12(b), where the depletion has been measured for different G_0 and probe power levels. Experimental results verify that the level of pump depletion in coded BOTDA depends not only on the probe power as the case of single-pulse BOTDA, but also on the level of G_0.

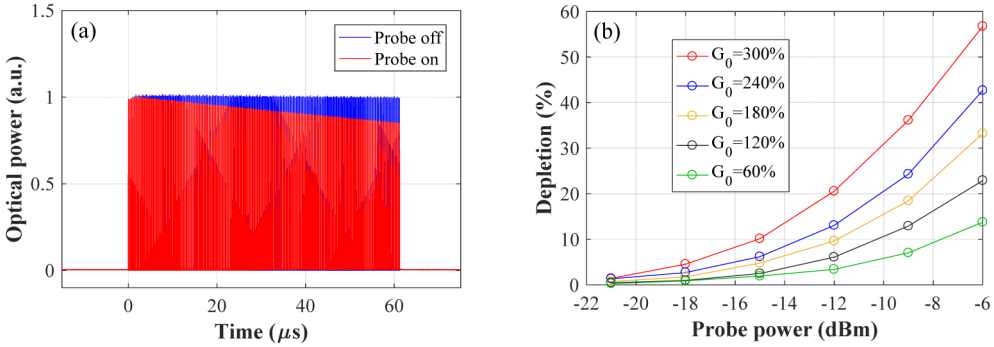

Fig. 12. (a) Experimentally measured code sequence power distribution when turning on and off the probe wave. (b) Depletion level of the last coded pulse as a function of the input probe power in cases of different G_0.

The impact of this cascaded pump depletion effect on the retrieved BFS profile is experimentally evaluated in a Simplex coded BOTDA sensor using 2-m spatial resolution and a 47 km-long sensing fiber. A 10 m-long hotspot has been induced close to the far fiber end, with a temperature difference of 25°C above room temperature. This is close to the condition corresponding to the maximum BFS error induced by non-local effect [31]. By adjusting the combination of both pump and probe powers, BFS profiles are retrieved under different depletion levels (20%, 10%, and 5%) of last coding pulse, as shown in Fig. 13. A reference BFS profile (grey curve) is also obtained using single-pulse BOTDA for comparison. Results show that an error in the hotspot BFS is induced due to depletion. This BFS error increases with the depletion level, resulting in 1.3 MHz error for a depletion of 20% of the last coding pulse. Since along the coding sequence the first coded pulse is negligibly depleted, while the last one experiences the strongest depletion level d, in average the equivalent depletion level for the whole coding sequence can be estimated to be $d/2$. This indicates that the BFS error in a coded BOTDA sensor is reduced to half compared to a single-pulse system with the same (maximum) depletion level.

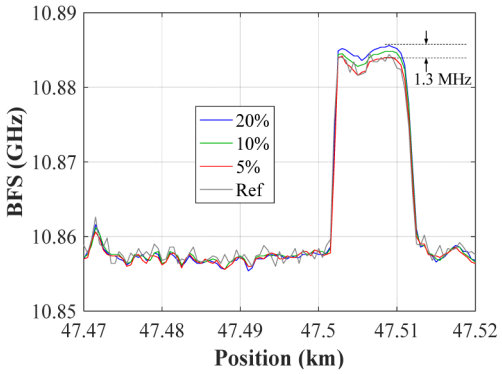

Fig. 13. BFS profiles measured around a hot-spot, obtained using single-pulse BOTDA and Simplex coded BOTDA with 20%, 10% and 5% depletion of the last coded pulse, respectively.

Defining the maximum tolerated BFS error determines the maximum depletion level d that is allowed in the system. This d in turn limits the maximum probe power per sideband

Optics EXPRESS

that can be launched into the sensing fiber for a certain G_0. This maximum probe power can be calculated based on Eq. (12) as:

$$P_{iS}^{\max}(G_0,d)=\frac{\ln(1-d)}{g_B(\nu)\left[\int_0^L f_{SU}(z)dz-\int_0^L f_{SL}(z)dz\right]} \tag{13}$$

The theoretical $P_{iS}^{\max}(G_0,d)$ calculated based on Eq. (13) for the cases of 10% (brown curve) and 20% (blue curve) depletions are shown in Fig. 14(a), with an ultimate probe power limit set to −6 dBm [5,6]. The theoretical curves agree well with the experimental results, validating the presented analysis.

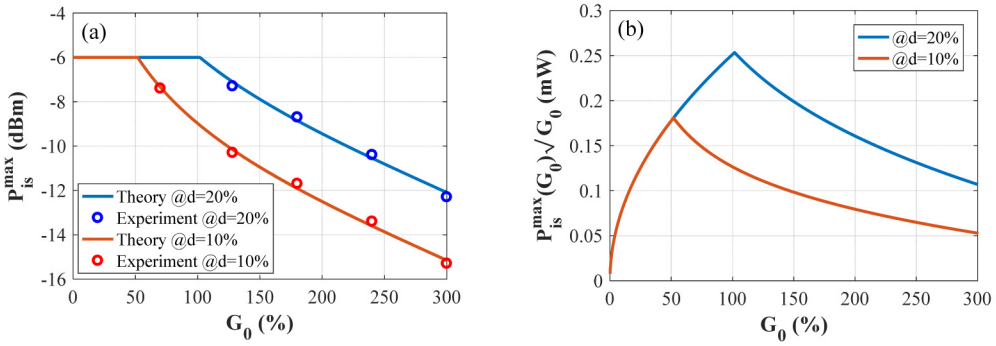

Fig. 14. (a) Maximum input probe power per sideband and (b) value of $P_{iS}^{\max}(G_0)\sqrt{G_0}$, both versus the accumulated Brillouin amplification in the cases of d = 20% and d = 10% depletion.

Knowing the maximum tolerable probe power for given G_0 and d allows evaluating the SNR performance of a unipolar coded BOTDA system. For a given code length M, the maximum SNR level is proportional to the maximum probe power, the decoded single-pulse Brillouin amplification $g_s = 2G_0/M$ and the SNR improvement from the coding gain $\sqrt{M}/2$:

$$SNR_{coded}^{\max}(G_0,d,M)\propto\frac{\sqrt{M}}{2}\frac{2G_0}{M}P_{iS}^{\max}(G_0,d)=\frac{P_{iS}^{\max}(G_0,d)G_0}{\sqrt{M}} \tag{14}$$

Equation (14) points out that in order to optimize the SNR performance in unipolar coded BOTDA systems, the code length M should be minimized for a given G_0 value. This means that g_s must be maximized, thus leading to:

$$M_{\min}=\frac{2G_0}{g_s^{\max}} \tag{15}$$

where $g_s^{\max}$ is the maximized single-pulse Brillouin gain. This suggests that the peak power of each pulse must be set as maximum (~100 mW in long fibers) for a given spatial resolution. Under this condition, the maximum SNR performance can be obtained by substituting Eq. (15) into Eq. (14):

$$SNR_{coded}^{\max}(G_0,d)\propto\frac{P_{iS}^{\max}(G_0,d)G_0}{\sqrt{M_{\min}}}=P_{iS}^{\max}(G_0,d)\sqrt{G_0}\sqrt{\frac{g_s^{\max}}{2}} \tag{16}$$

Then, the ultimate SNR improvement $\Delta SNR^{\max}$ brought by unipolar codes over an optimized single-pulse BOTDA can be readily derived. In single-pulse BOTDA, the optimal

Optics EXPRESS

SNR, $SNR_{pulse}^{\max}$, is proportional to the maximum single-pulse Brillouin amplification $g_s^{\max}$ and the maximum probe power ($P_{iS-pulse}^{\max} = -6$ dBm):

$$SNR_{pulse}^{\max} \propto P_{iS-pulse}^{\max} g_s^{\max} \tag{17}$$

Thus, $\Delta SNR^{\max}$ is given by the ratio between Eq. (16) and Eq. (17):

$$\Delta SNR^{\max}(G_0, d) = \frac{SNR_{coded}^{\max}}{SNR_{pulse}^{\max}} = \frac{P_{iS}^{\max}(G_0, d)\sqrt{G_0}}{P_{iS-pulse}^{\max}\sqrt{2g_s^{\max}}} \tag{18}$$

Since in the optimized single-pulse case, the denominator of Eq. (18) is constant, the SNR improvement basically depends on the term $P_{iS}^{\max}(G_0, d)\sqrt{G_0}$. For the sake of visual clarity, the behavior of this term as a function of G_0 is illustrated in Fig. 14(b), for different d. The figure clearly indicates that the maximum SNR of a coded BOTDA sensor can be achieved at very specific values of G_0. For example, a depletion level of 20% corresponds to an optimal G_0 equal to 1 (100%), as illustrated in Fig. 14(b). Considering that this case corresponds to the maximum tolerable depletion level (corresponding to 1.3 MHz BFS estimation error due to higher-order non-local effects), Eq. (18) can be simplified as:

$$\Delta SNR^{\max} = \frac{1}{\sqrt{2g_s^{\max}}} \tag{19}$$

with an optimized M equal to $2/g_s^{\max}$ according to Eq. (15). Note that Eq. (19) emphasizes that the optimal SNR improvement given by unipolar codes solely depends on $g_s^{\max}$, which is ultimately determined by the spatial resolution since the pulse peak power must always be kept at its maximum level (~100 mW). This indicates that the wider the spatial resolution, the larger $g_s^{\max}$ that leads to the lower SNR improvement when using unipolar coded BOTDA. Therefore, when Eq. (19) is equal to or smaller than 1, which is calculated as corresponding to the case of $g_s^{\max} \geq 50\%$ (spatial resolution ≥ 30 m), the unipolar coding technique has no benefit with respect to an ultimately optimized single-pulse BOTDA system.

Note that Eq. (19) is valid provided that M is equal to its minimal value, i.e., rounded-off from $2/g_s^{\max}$, which in principle can take any integer value. This condition can be fulfilled for instance by using unipolar Cyclic coding. For a BOTDA system with a $g_s^{\max}$ of 1%, which typically corresponds to 1 or 2 m spatial resolution, the optimum coding length is ~200 bits and the maximum SNR improvement benefiting from the cyclic coding technique is 8 dB according to Eq. (19), in agreement with the expected coding gain. However, in other more general cases, such as the conventional unipolar unicolor Simplex and Golay coding, the coding lengths must be 2^n-1 and 2^n, respectively. In such situation the value of n has to be optimized, to ensure that M (equal to 2^n-1 or 2^n) is the closest possible to the optimal value (e.g., $M = 2/g_s^{\max}$ for the case of 20% depletion). Taking into account the Simplex coded BOTDA system in our experiment, where the value of $g_s^{\max}$ is 1.2% for 2-m spatial resolution, the corresponding optimal n in practice is equal to 7 (i.e., optimal M = 127 bits), which gives rise to a theoretical $\Delta SNR^{\max}$ = 7.5 dB. This value is indeed in good agreement with the experimental result, thus validating the presented theoretical analysis.

8. Conclusion

In summary, critical factors affecting the performance of unicolor unipolar coded BOTDA have been thoroughly evaluated. The presented study suggests solutions and quantitatively

Optics EXPRESS

defines the optimal working conditions, providing the following design rules to enable distortion-free unipolar-coded BOTDA sensing operating at the highest SNR:

1) Before performing the linear decoding process, the linear accumulated Brillouin amplification must be retrieved using the proposed logarithmic normalization.

2) For long-range unipolar-coded BOTDA, Simplex coding is preferred (compared to unipolar Golay coding) due to its robustness against pulse power non-uniformity.

3) To eliminate polarization fading in the decoded Brillouin gain traces, the use of a polarization scrambler is suggested (instead of polarization switch), since it can greatly alleviate the polarization pulling resulting from long pulse coding sequences.

4) Due to the limitation imposed by higher-order non-local effects, the ideal code length must be close to $2/g_s^{\max}$.

Following these design rules, a maximum SNR improvement of $1/\sqrt{2g_s^{\max}}$ can be attained when compared to an optimized single-pulse BOTDA system. This brings on the essential novel result that the best advantage from coding is obtained in situations when the single pulse gain is small, i.e., for short spatial resolutions (2 meter and less).

Note that although higher-order non-local effect is identified as the most relevant factor limiting the performance of unipolar coded BOTDA systems, there also exist some alternatives to partially overcome this limitation. For instance, reducing the probe power significantly can allow for the use of longer code sequences, while the reduced SNR (due to probe power reduction) can be partially recovered by using pre-amplification in front of the receiver. Another alternative is the use of colored (time-frequency) or bipolar codes, since in those cases the Brillouin interaction along the entire sensing fiber is highly reduced, thus mitigating cascaded pump depletion effects. Although a procedure for optimizing only unipolar coded BOTDA sensors has been presented in this paper, similar procedure and strategies can be derived for those other types of codes.

Funding

Swiss Commission for Technology and Innovation (18337.2 PFNM-NM); China Scholarship Council (CSC).